Scattering Matrix Integral Equation Analysis for the Design of a Waveguide Rotman Lens

Andrew F. Peterson, *Senior Member, IEEE*, and Ekkehart O. Rausch

***Abstract*— An integral-equation-based procedure is developed for determining the scattering parameters of a multiport Rotman lens device. The device is intended for use at millimeter-wave frequencies and incorporates rectangular waveguide feeds. The integral equation model takes higher order modes in the feed apertures into account and incorporates mutual coupling between neighboring ports. A prototype lens was designed using the integral equation model and fabricated. The lens S-parameters were measured and modified with an ideal -40 dB $(n = 3)$ Taylor weighting function. The resulting beam sidelobe level is better than -30 dB.**

***Index Terms*— Rotman lens.**

I. Introduction

ELECTRONICALLY steered millimeter-wave antennas have numerous applications including radar, communication systems, synthetic vision schemes for weapon detection, and collision avoidance systems for automobiles. Traditional phased-array antennas are high in cost due to phase shifters. A less expensive antenna, based on a Rotman lens, offers a rugged, reliable, and compact alternative to current millimeter-wave electronically scanned antenna technologies. Traditional Rotman lens designs can be carried out following [1]–[3]. These lenses incorporate TEM propagation and exhibit relatively wide bandwidths (typically 3 : 1 or better). At millimeter-wave frequencies, dielectric losses and small physical dimensions complicate a TEM lens realization. One possibility is to adopt a non-TEM parallel-plate mode of propagation which limits the bandwidth but makes it convenient to incorporate rectangular waveguide feeds around the lens periphery. Such a lens was recently fabricated and tested at 37 GHz [4]. The Rotman design equations do not specify the shape of the sidewall that joins the lens focal ports to the lens array ports, and while they specify the port locations they do not specify the port widths. These parameters can substantially affect the lens performance, especially the sidelobe level and insertion loss. In order to evaluate various lens designs, and to determine the effect of mutual coupling on the lens performance, a numerical model was developed to predict the N-port scattering matrix. The following describes the analysis procedure used to characterize the device.

Manuscript received March 15, 1998; revised January 24, 1999.

A. F. Peterson is with the School of Electrical and Computer Engineering, Georgia Institute of Technology, Atlanta, GA 30332 USA.

E. O. Rausch is with the Georgia Tech Research Institute, Georgia Institute of Technology, Atlanta, GA 30332 USA.

Publisher Item Identifier S 0018-926X(99)04833-4.

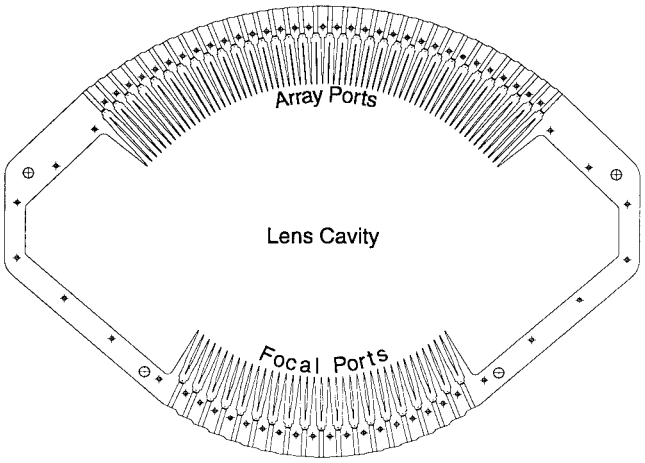

Fig. 1. Cross section of a waveguide Rotman lens geometry.

A cross-sectional view of the Rotman lens geometry under consideration is shown in Fig. 1. Rectangular waveguide feed lines are used to route the signals between the input and output ports and the lens cavity. To lower the sidelobe level within the scan angle, an aperture-to-aperture separation of less than half a wavelength in the air-filled lens cavity is desired. Therefore, the waveguides are oriented with their broad wall vertical, so that the electric field of the dominant rectangular waveguide mode is parallel to the conducting planes of the lens cavity. Consequently, the electric field within the lens cavity is polarized horizontally, in contrast to a traditional TEM lens design. The waveguides are tapered along their transverse dimension near the lens cavity to provide a gradual transition and an improved impedance match at the apertures, which are located along the lens cavity boundary. In the particular design under consideration, a folded magic tee was incorporated in each feed line to provide a 3-dB power divider, which split the feeds into two smaller in-phase apertures. Along the sides of the lens (Fig. 1), dummy ports may be introduced to fill out the contour, or absorber material may be placed in the lens ears to reduce reflections. A convenient description of the N-port device can be obtained in terms of a scattering matrix (S-matrix), which relates the complex-valued input and output signals at a single frequency [5]. Essentially, every aspect of the lens performance can be evaluated from the S-matrix.

The formulation is based on a generalization of planar circuit analysis [6], [7]. In planar circuit analysis, the electric and magnetic fields within microstrip or stripline devices are assumed to be invariant with respect to z (their thin

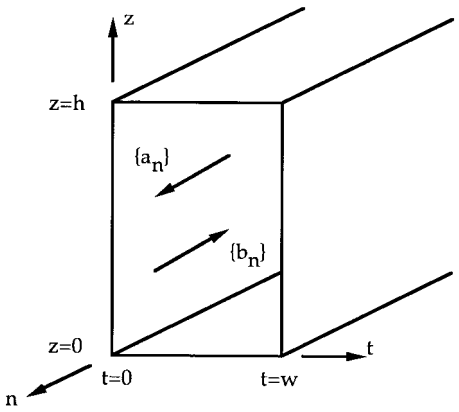

Fig. 2. Coordinate system used in the rectangular waveguide ports. The direction indicated by the variable n points toward the lens interior.

dimension) which permits these devices to be modeled as two-dimensional structures. One approach is to introduce a two-dimensional integral equation relating the electric and magnetic fields around the outer contour of the structure. TEM Rotman lenses were modeled this way by Chan [8] and Sharma *et al.* [9]. Chan's approach offered the improvement of using waveguide-like modes in the lens feeds, enhancing the efficiency of analysis. A similar approach was adapted by the authors in earlier work involving microstrip and stripline TEM lenses [10]–[12]. In the present work, the z dependence of all fields of interest is a half-sinusoid corresponding to the first higher order parallel-plate waveguide mode. Planar circuit analysis can be generalized to incorporate this z dependence.

The analysis procedure involves a traditional modal expansion within the rectangular waveguide feed lines, and utilizes expressions for the electromagnetic fields radiated from the aperture of a waveguide into the lens cavity (which is modeled as a parallel-plate waveguide). The contributions from each mode in each waveguide aperture are combined into an integral equation. The discrete form of the integral equation can be rewritten in matrix form, producing a generalized scattering matrix. The generalized S-matrix contains information about the primary (dominant) waveguide modes, as well as higher order waveguide modes. Finally, information about the behavior of higher order waveguide modes in the tapered feed lines is used to reduce the generalized scattering matrix to an ordinary scattering matrix involving only the dominant modes.

The following sections describe the notation we use for the waveguide modes, the scattering matrix, and the integral equation formulation. The incorporation of lossy absorbing material into the lens is summarized, and the procedure used to reduce the S-matrix to dominant modes is delineated. Finally, numerical results are compared with measurements carried out on a prototype millimeter-wave lens.

II. Formulation

Fig. 2 shows the local coordinate system used for each rectangular waveguide feed. The electromagnetic fields that exist in the guide can be decomposed into a superposition of modes. Since the vertical dimension of the lens geometry is uniform, we consider only TE_{1m} modes, which are TE modes with a single half-sinusoidal variation in the vertical (z) direction [5]. We also assume that there are incident and reflected modes in each feed line. Using the (n, t, z) coordinate system from Fig. 2, the tangential electric fields in each waveguide aperture can be written as

$$E_t(n,t,z) = \sum_{m=0}^{M-1} \{a_m e^{-j\beta_m n} + b_m e^{j\beta_m n}\} Q_m \sin\left(\frac{\pi z}{h}\right) \cdot \cos\left(\frac{m\pi t}{w}\right) \tag{1}$$

$$E_z(n,t,z) = -\sum_{m=0}^{M-1} \{a_m e^{-j\beta_m n} + b_m e^{j\beta_m n}\} Q_m \left(\frac{mh}{w}\right) \cdot \cos\left(\frac{\pi z}{h}\right) \sin\left(\frac{m\pi t}{w}\right) \tag{2}$$

and the components of the tangential magnetic field can be written

$$H_t(n,t,z) = \sum_{m=0}^{M-1} \{a_m e^{-j\beta_m n} - b_m e^{j\beta_m n}\} \frac{Q_m}{Z_m} \left(\frac{m\pi}{2}\right) \cdot \cos\left(\frac{\pi z}{h}\right) \sin\left(\frac{m\pi t}{w}\right) \tag{3}$$

$$H_z(n,t,z) = \sum_{m=0}^{M-1} \{a_m e^{-j\beta_m n} - b_m e^{j\beta_m n}\} \frac{Q_m}{Z_m} \left(\frac{\pi w}{2h}\right) \cdot \sin\left(\frac{\pi z}{h}\right) \cos\left(\frac{m\pi t}{w}\right) \tag{4}$$

where h denotes the vertical (z) waveguide dimension, w the horizontal (transverse) dimension

$$Q_m = \sqrt{\frac{4\varepsilon_m Z_m}{\pi(w^2 + m^2 h^2)}} \tag{5}$$

$$\varepsilon_m = \begin{cases} 1, & m = 0 \\ 2, & m > 0 \end{cases} \tag{6}$$

$$\beta_m = \begin{cases} \sqrt{\omega^2\mu\varepsilon - \left(\frac{\pi}{h}\right)^2 - \left(\frac{m\pi}{w}\right)^2}, \\ \qquad \omega^2\mu\varepsilon > \left(\frac{\pi}{h}\right)^2 + \left(\frac{m\pi}{w}\right)^2 \\ -j\sqrt{\left(\frac{\pi}{h}\right)^2 + \left(\frac{m\pi}{w}\right)^2 - \omega^2\mu\varepsilon}, \\ \qquad \text{otherwise} \end{cases} \tag{7}$$

and Z_m is the pseudocharacteristic impedance of the TE_{1m} mode defined by

$$Z_m = \frac{\pi w}{2h} \frac{\omega\mu}{\beta_m}. \tag{8}$$

The parameters $\{a_m\}$ denote the complex-valued coefficients associated with the modes propagating toward the lens interior while the set $\{b_m\}$ denotes the coefficients associated with the modes propagating away from the lens interior (Fig. 2). The normalization provided in (1)–(4) scales the fields so that the

power carried by a propagating mode is given by

$$\int_{z=0}^{h}\int_{t=0}^{w}\frac{1}{2}\,\mathrm{Re}\{\overline{E}\times\overline{H}^{*}\}\,dt\,dz=\hat{n}\frac{|a_m|^2}{2}. \tag{9}$$

This corresponds to a wave amplitude proportional to the square root of power, as normally used with scattering parameters [5].

We seek a description of the lens in terms of the incident and reflected modes, and define the generalized scattering matrix according to

$$\begin{bmatrix} b_1 \\ b_2 \\ \vdots \\ b_{NM} \end{bmatrix} = \begin{bmatrix} S_{11} & S_{12} & \cdots & S_{1,\,NM} \\ S_{21} & S_{22} & & \\ \vdots & & & \\ S_{NM,\,1} & & \cdots & S_{NM,\,NM} \end{bmatrix} \begin{bmatrix} a_1 \\ a_2 \\ \vdots \\ a_{NM} \end{bmatrix} \tag{10}$$

where we have assumed that there are N apertures around the lens periphery, each containing M modes. The coefficients $\{a_n\}$ and $\{b_n\}$ are defined at specific reference planes within each waveguide [5]. Initially in the analysis to follow, the reference planes will be located in the apertures of the guides (at the lens cavity boundary). As the final step in the analysis, the reference planes are shifted down the waveguides to the connectors (to facilitate a comparison with measured S-parameter data).

The scattering matrix can be constructed from an integral equation constraining the waveguide aperture fields around the lens periphery. Initially, suppose that the entire periphery of the lens interior is surrounded by N apertures. We will use the index q to denote the source aperture, while p denotes the index of the observer aperture. As above, m is used to denote the index of the source mode. The coefficients a_m^q and b_m^q are those associated with the mth mode in the qth aperture. Because of the specific field components involved in this application it is convenient to develop an integral equation using the z-component of the magnetic field. The integral equation imposes the consistency condition that the total magnetic field in aperture p must be the same as the superposition of the radiated magnetic fields produced there by the various modes of all N waveguide apertures (including the self-contribution from aperture p). The z-component of the magnetic field in aperture p can be rewritten using (4) and (8) as

$$H_z^{\text{aperture}\,p}=\sum_{m=0}^{\infty}(a_m^p-b_m^p)Q_m^p\frac{\beta_m^p}{\omega\mu}\cos\left(\frac{m\pi u}{w^p}\right) \tag{11}$$

where u denotes a local variable defined in aperture p, and the various superscripts denote the aperture index associated with the parameters. For the purpose of calculating the radiated field due to a rectangular waveguide aperture, the fields in each aperture can be replaced by equivalent electric and magnetic currents [13]. The equivalent currents act as sources of the radiated field produced at other locations throughout the lens interior. The necessary currents are a transverse component of electric current and a z-component of magnetic current. For clarity, let us introduce the notation $\{hzjt_{qm}^p\}$ to denote the H field produced in aperture p by an electric current source in aperture q with sinusoidal variation m, and $\{hzmz_{qm}^p\}$ to denote the H field produced in aperture p by a magnetic current source in aperture q with sinusoidal variation m. (Expressions for these quantities are provided in the Appendix.) The magnetic field produced in aperture p by electromagnetic radiation from all the apertures (including p) can be written as

$$\begin{aligned} H_z^{\text{aperture}\,p} &= -\sum_{q=1}^{N}\sum_{m=0}^{\infty}(a_m^q-b_m^q)Q_m^q\frac{\beta_m^q}{\omega\mu}hzjt_{qm}^p(u) \\ &\quad -\sum_{q=1}^{N}\sum_{m=0}^{\infty}(a_m^q+b_m^q)Q_m^q\left(\frac{\beta_m^q}{k_{pp}}\right)^2 hzmz_{qm}^p(u) \end{aligned} \tag{12}$$

where

$$k_{pp}=\sqrt{k^2-\left(\frac{\pi}{h}\right)^2} \tag{13}$$

denotes the phase constant within the parallel-plate region. The condition that the total magnetic field in aperture p must be the same as the superposition of the radiated magnetic fields produced there by the various modes of all N waveguide apertures can be obtained by equating (11) and (12), to produce

$$\begin{aligned} &\sum_{m=0}^{\infty}(a_m^p-b_m^p)Q_m^p\frac{\beta_m^p}{\omega\mu}\cos\left(\frac{m\pi u}{w^p}\right) \\ &\quad=-\sum_{q=1}^{N}\sum_{m=0}^{\infty}(a_m^q-b_m^q)Q_m^q\frac{\beta_m^q}{\omega\mu}hzjt_{qm}^p(u) \\ &\qquad-\sum_{q=1}^{N}\sum_{m=0}^{\infty}(a_m^q+b_m^q)Q_m^q\left(\frac{\beta_m^q}{k_{pp}}\right)^2 hzmz_{qm}^p(u). \end{aligned} \tag{14}$$

In principle, (14) provides a complete description of the electromagnetic interactions occurring within the lens. If we separate the coefficients of incoming and outgoing waves in each guide, this equation is equivalent to

$$\begin{aligned} &\sum_{m=0}^{\infty}b_m^pQ_m^p\frac{\beta_m^p}{\omega\mu}\cos\left(\frac{m\pi u}{w^p}\right)+\sum_{q=1}^{N}\sum_{m=0}^{\infty}b_m^qQ_m^q\frac{\beta_m^q}{\omega\mu}hzjt_{qm}^p(u) \\ &\qquad-\sum_{q=1}^{N}\sum_{m=0}^{\infty}b_m^qQ_m^q\left(\frac{\beta_m^q}{k_{pp}}\right)^2 hzmz_{qm}^p(u) \\ &\quad=\sum_{m=0}^{\infty}a_m^pQ_m^p\frac{\beta_m^p}{\omega\mu}\cos\left(\frac{m\pi u}{w^p}\right) \\ &\qquad+\sum_{q=1}^{N}\sum_{m=0}^{\infty}a_m^qQ_m^q\frac{\beta_m^q}{\omega\mu}hzjt_{qm}^p(u) \\ &\qquad+\sum_{q=1}^{N}\sum_{m=0}^{\infty}a_m^qQ_m^q\left(\frac{\beta_m^q}{k_{pp}}\right)^2 hzmz_{qm}^p(u). \end{aligned} \tag{15}$$

NM linearly independent equations can be extracted from (15) by first truncating the upper limit of the index m to $M-1$,

and then integrating each term with the testing function

$$\cos\left(\frac{v\pi u}{w^p}\right) \tag{16}$$

where v is the index of the test mode in aperture p ($0 \le v \le M-1$). The resulting system of equations has the form

$$\begin{aligned}
&\sum_{m=0}^{M-1} b_m^p Q_m^p \frac{\beta_m^p}{\omega\mu} \int_{u=0}^{w^p} \cos\left(\frac{v\pi u}{w^p}\right) \cos\left(\frac{m\pi u}{w^p}\right) du \\
&\quad + \sum_{q=1}^{N} \sum_{m=0}^{M-1} b_m^q Q_m^q \frac{\beta_m^q}{\omega\mu} hzjt_{qm}^{pv} \\
&\quad - \sum_{q=1}^{N} \sum_{m=0}^{M-1} b_m^q Q_m^q \left(\frac{\beta_m^q}{k_{pp}}\right)^2 hzmz_{qm}^{pv} \\
&= \sum_{m=0}^{M-1} a_m^p Q_m^p \frac{\beta_m^p}{\omega\mu} \int_{u=0}^{w^p} \cos\left(\frac{v\pi u}{w^p}\right) \cos\left(\frac{m\pi u}{w^p}\right) du \\
&\quad + \sum_{q=1}^{N} \sum_{m=0}^{M-1} a_m^q Q_m^q \frac{\beta_m^q}{\omega\mu} hzjt_{qm}^{pv} \\
&\quad + \sum_{q=1}^{N} \sum_{m=0}^{M-1} a_m^q Q_m^q \left(\frac{\beta_m^q}{k_{pp}}\right)^2 hzmz_{qm}^{pv}
\end{aligned} \tag{17}$$

where $\{hzjt_{qm}^{pv}\}$ and $\{hzmz_{qm}^{pv}\}$ are defined in the obvious manner, i.e.,

$$hzjt_{qm}^{pv} = \int_{u=0}^{w^p} \cos\left(\frac{v\pi u}{w^p}\right) hzjt_{qm}^{p}(u)\, du. \tag{18}$$

Explicit expressions for $\{hzjt_{qm}^{pv}\}$ and $\{hzmz_{qm}^{pv}\}$ are given in the Appendix. The system of equations can be organized in matrix form as

$$\boldsymbol{U}\boldsymbol{b} = \boldsymbol{T}\boldsymbol{a} \tag{19}$$

where $\boldsymbol{U}$ and $\boldsymbol{T}$ are $NM \times NM$ matrices, and $\boldsymbol{a}$ and $\boldsymbol{b}$ are column vectors containing the coefficients $\{a_m^q\}$ and $\{b_m^q\}$. The entries of $\boldsymbol{U}$ are

$$\begin{aligned}
\boldsymbol{U}_{pv,\,qm} &= Q_m^p \frac{\beta_m^p}{\omega\mu} \int_{u=0}^{w^p} \cos\left(\frac{v\pi u}{w^p}\right) \cos\left(\frac{m\pi u}{w^p}\right) du \\
&\quad + Q_m^q \frac{\beta_m^q}{\omega\mu} hzjt_{qm}^{pv} - Q_m^q \left(\frac{\beta_m^q}{k_{pp}}\right)^2 hzmz_{qm}^{pv}
\end{aligned} \tag{20}$$

if $p = q$ and

$$\boldsymbol{U}_{pv,\,qm} = Q_m^q \frac{\beta_m^q}{\omega\mu} hzjt_{qm}^{pv} - Q_m^q \left(\frac{\beta_m^q}{k_{pp}}\right)^2 hzmz_{qm}^{pv} \tag{21}$$

if p and q differ. The entries of $\boldsymbol{T}$ are

$$\begin{aligned}
\boldsymbol{T}_{pv,\,qm} &= Q_m^p \frac{\beta_m^p}{\omega\mu} \int_{u=0}^{w^p} \cos\left(\frac{v\pi u}{w^p}\right) \cos\left(\frac{m\pi u}{w^p}\right) du \\
&\quad + Q_m^p \frac{\beta_m^q}{\omega\mu} hzjt_{qm}^{pv} + Q_m^q \left(\frac{\beta_m^q}{k_{pp}}\right)^2 hzmz_{qm}^{pv}
\end{aligned} \tag{22}$$

if $p = q$ and

$$\boldsymbol{T}_{pv,\,qm} = Q_m^p \frac{\beta_m^q}{\omega\mu} hzjt_{qm}^{pv} + Q_m^q \left(\frac{\beta_m^q}{k_{pp}}\right)^2 hzmz_{qm}^{pv} \tag{23}$$

if p and q differ. These entries can be obtained by a numerical evaluation of the necessary integrals as defined in the Appendix.

Once the matrices $\boldsymbol{T}$ and $\boldsymbol{U}$ are constructed, the generalized scattering matrix defined in (10) can be obtained from

$$\boldsymbol{b} = \boldsymbol{S}\boldsymbol{a} = \boldsymbol{U}^{-1}\boldsymbol{T}\boldsymbol{a} \tag{24}$$

and has dimension $NM \times NM$. This matrix will be processed to reduce its dimension to $N \times N$, as described in the following sections.

III. Incorporation of Absorbing Material

The presence of lossy absorbing material along a portion of the periphery of the lens interior can be taken into account in several ways. For simplicity, we assume that the field components at the surface of the absorber are entirely of the TE_1 parallel-plate mode, and that they satisfy the impedance boundary condition

$$E_t = -\eta_s H_z \tag{25}$$

where η_s is the surface impedance of the absorbing material. An absorber with minimal reflections should have a surface impedance that is a good match to the parallel-plate TE_1 wave impedance, which suggests a value close to

$$\eta_s = \omega\mu/k_{pp} \tag{26}$$

as the surface impedance for a "good" absorber.

Over the region containing the absorber, the tangential fields (H_z and E_t) can be replaced by equivalent sources ($-J_t$ and $-M_z$). These sources, which are unknown quantities that are related to each other by (25), radiate to produce the reflected fields throughout the lens interior. The absorber contour can be divided into cells, and the equivalent sources can be represented by an expansion in basis functions. For simplicity, we consider piecewise-constant functions, which have the same transverse dependence as the $m = 0$ rectangular waveguide mode. The integral equation is modified to incorporate the additional unknowns associated with the absorber region, which produces additional terms in (14), (15), and (17). Since the sources have the same dependence as the $m = 0$ rectangular waveguide mode, the fields produced by these sources can be obtained using the same expressions as the aperture sources. In this case we use the coefficients $\{c_i\}$ to represent the electric current density J_t, and replace M_z with the equivalent quantity $-\eta_s J_t$. The coefficients $\{c_i\}$ are actually eliminated from the system and do not need to be determined by the analysis procedure.

Therefore, by imposing the consistency condition that the magnetic field in aperture p equals the sum of all the radiated fields produced there, (15) can be rewritten as

$$\begin{aligned}
&\sum_{m=0}^{M-1} b_m^p Q_m^p \frac{\beta_m^p}{\omega\mu} \cos\left(\frac{m\pi u}{w^p}\right) \\
&\quad + \sum_{q=1}^{N}\sum_{m=0}^{M-1} b_m^q Q_m^q \frac{\beta_m^q}{\omega\mu} hzjt_{qm}^p(u) \\
&\quad - \sum_{q=1}^{N}\sum_{m=0}^{M-1} b_m^q Q_m^q \left(\frac{\beta_m^q}{k_{pp}}\right)^2 hzmz_{qm}^p(u) \\
&= \sum_{m=0}^{M-1} a_m^p Q_m^p \frac{\beta_m^p}{\omega\mu} \cos\left(\frac{m\pi u}{w^p}\right) \\
&\quad + \sum_{q=1}^{N}\sum_{m=0}^{M-1} a_m^q Q_m^q \frac{\beta_m^q}{\omega\mu} hzjt_{qm}^p(u) \\
&\quad + \sum_{q=1}^{N}\sum_{m=0}^{M-1} a_m^q Q_m^q \left(\frac{\beta_m^q}{k_{pp}}\right)^2 hzmz_{qm}^p(u) \\
&\quad - \sum_{i=1}^{L} c_i hzjt_{i0}^p(u) + \sum_{i=1}^{L} \eta_s c_i hzmz_{i0}^p(u) \qquad (27)
\end{aligned}$$

where the additional summations over the index $\{i\}$ represent the contributions from the L absorber cells. If the equation is integrated with the testing function in (16), for $0 \le v \le M-1$, the resulting system can be organized in matrix form according to

$$\boldsymbol{U}\boldsymbol{b} = \boldsymbol{T}\boldsymbol{a} + \boldsymbol{Z_{ap}}\boldsymbol{c} \qquad (28)$$

where $\boldsymbol{U}$ and $\boldsymbol{T}$ are square matrices of dimension NM, and $\boldsymbol{Z_{ap}}$ is a rectangular matrix of dimension $NM \times L$. A similar equation can be written in each of the absorber cells, and placed in the form

$$\boldsymbol{Z_U}\boldsymbol{b} = \boldsymbol{Z_T}\boldsymbol{a} + \boldsymbol{Z_{ab}}\boldsymbol{c} \qquad (29)$$

where $\boldsymbol{Z_U}$, and $\boldsymbol{Z_T}$ are rectangular matrices of dimension $L \times NM$ and $\boldsymbol{Z_{ab}}$ is a square matrix of dimension L. The $L \times 1$ column vector $\boldsymbol{c}$ contains the coefficients of the absorber basis functions. The entries of $\boldsymbol{U}$ and $\boldsymbol{T}$ are the same as in the preceding section, and the other entries are given by

$$(\boldsymbol{Z_{ap}})_{pv,i} = -hzjt_{i0}^{pv} + \eta_s hzmz_{i0}^{pv} \qquad (30)$$

$$(\boldsymbol{Z_U})_{h,mq} = Q_m^q \frac{\beta_m^q}{\omega\mu} hzjt_{qm}^{h0} - Q_m^q \left(\frac{\beta_m^q}{k_{pp}}\right)^2 hzmz_{qm}^{h0} \qquad (31)$$

$$(\boldsymbol{Z_T})_{h,mq} = Q_m^q \frac{\beta_m^q}{\omega\mu} hzjt_{qm}^{h0} + Q_m^q \left(\frac{\beta_m^q}{k_{pp}}\right)^2 hzmz_{qm}^{h0}. \qquad (32)$$

The off-diagonal entries of $\boldsymbol{Z_{ab}}$ are given by

$$(\boldsymbol{Z_{ab}})_{h,i} = -hzjt_{i0}^{h0} + \eta_s hzmz_{i0}^{h0} \qquad (33)$$

while the diagonal entries are

$$(\boldsymbol{Z_{ab}})_{h,h} = -w^h - hzjt_{h0}^{h0} + \eta_s hzmz_{h0}^{h0} \qquad (34)$$

where w^h is the width of the hth cell along the absorber.

Equation (29) can be inverted to produce

$$\boldsymbol{c} = \boldsymbol{Z_{ab}^{-1}}\boldsymbol{Z_U}\boldsymbol{b} - \boldsymbol{Z_{ab}^{-1}}\boldsymbol{Z_T}\boldsymbol{a} \qquad (35)$$

and used to eliminate the coefficients $\{c_n\}$ from (28), to leave

$$(\boldsymbol{U} - \boldsymbol{Z_{ap}}\boldsymbol{Z_{ab}^{-1}}\boldsymbol{Z_U})\boldsymbol{b} = (\boldsymbol{T} - \boldsymbol{Z_{ap}}\boldsymbol{Z_{ab}^{-1}}\boldsymbol{Z_T})\boldsymbol{a}. \qquad (36)$$

Finally, the $NM \times NM$ generalized scattering matrix is obtained from

$$\boldsymbol{b} = \boldsymbol{S}\boldsymbol{a} = (\boldsymbol{U} - \boldsymbol{Z_{ap}}\boldsymbol{Z_{ab}^{-1}}\boldsymbol{Z_U})^{-1}(\boldsymbol{T} - \boldsymbol{Z_{ap}}\boldsymbol{Z_{ab}^{-1}}\boldsymbol{Z_T})\boldsymbol{a}. \qquad (37)$$

The additional matrix manipulations needed to construct the $NM \times NM$ system in (37) account for the energy lost to the absorbing material. The extra matrix entries can be obtained using the same subroutines used to produce the entries of $\boldsymbol{U}$ and $\boldsymbol{T}$ for (24).

IV. Reduction to an Ordinary Scattering Matrix

In a practical lens configuration, the higher order modes excited in the apertures of the various ports do not propagate beyond the tapered transition to a single-mode waveguide. Thus these modes carry no net energy away from the lens, and can be eliminated from the generalized S-matrix (by a procedure that accounts for their presence). In the process, the generalized scattering matrix of order NM is reduced to an ordinary $N \times N$ scattering matrix.

The elimination procedure requires the complex-valued reflection coefficient Γ associated with each higher order mode as seen "looking into" the tapered transition from the aperture, which provides an auxiliary relationship between the mode coefficients of the form

$$a_i = \Gamma b_i. \qquad (38)$$

The reflection coefficient is a function of the geometry of the tapered guide, and can be determined for a particular mode from knowledge of the impedance as a function of position.

For this study, we use (8) to define the characteristic impedance of a tapered waveguide as a function of width. To calculate the reflection coefficient, we use a numerical procedure that replaces the continuous tapered guide by a cascaded collection of uniform waveguides, each having a different impedance in order to achieve a "staircase approximation" of the true impedance function (Fig. 3). The reflection coefficient of the cascaded arrangement is computed using standard transmission line or waveguide theory. For the tapers considered in this study, a number of subdivisions exceeding about 200 produce reflection coefficients stable to machine precision (i.e., there was no further change in the reflection coefficient with additional subdivisions).

Once the reflection coefficient Γ is determined for the first few modes associated with each waveguide, (38) provides a constraint that can be used to eliminate one row and column of the generalized S-matrix. Suppose that the index i represents the very last entry in the generalized S-matrix. In other words,

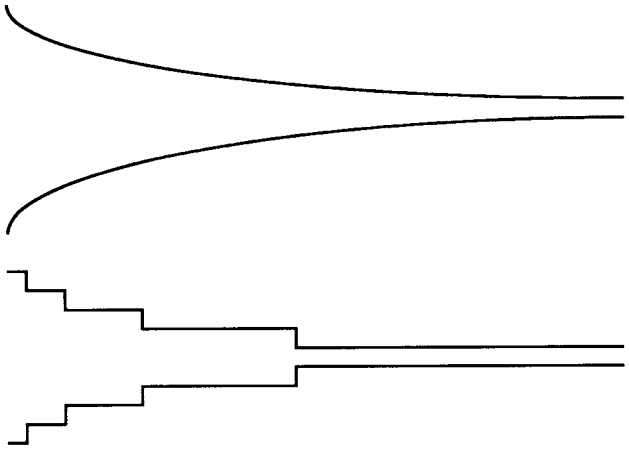

Fig. 3. Tapered waveguide cross section and the cascaded sections of uniform guide actually used to determine the reflection coefficients. The actual calculations employed 200 divisions of uniform length to approximate the curved taper.

(10) can be rewritten as

$$\begin{bmatrix} b_1 \\ b_2 \\ \vdots \\ b_i \end{bmatrix} = \begin{bmatrix} S_{11} & S_{12} & \cdots & S_{1i} \\ S_{21} & S_{22} & & \\ \vdots & & & \\ S_{i1} & & \cdots & S_{ii} \end{bmatrix} \begin{bmatrix} a_1 \\ a_2 \\ \vdots \\ a_i \end{bmatrix}. \tag{39}$$

After substituting (38) into (39), the S-matrix has the form

$$\begin{bmatrix} b_1 \\ b_2 \\ \vdots \\ b_i \end{bmatrix} = \begin{bmatrix} S_{11} & S_{12} & \cdots & S_{1,i-1} \\ S_{21} & S_{22} & & \\ \vdots & & & \\ S_{i1} & & \cdots & S_{i,i-1} \end{bmatrix} \begin{bmatrix} a_1 \\ a_2 \\ \vdots \\ a_{i-1} \end{bmatrix} + \begin{bmatrix} S_{1i}b_i\Gamma \\ S_{2i}b_i\Gamma \\ \vdots \\ S_{ii}b_i\Gamma \end{bmatrix}. \tag{40}$$

The ith equation can be solved for b_i to produce

$$b_i = \frac{S_{i1}a_1 + S_{i2}a_2 + \cdots + S_{i,i-1}a_{i-1}}{1 - S_{ii}\Gamma}. \tag{41}$$

Substituting this result back into the other rows of (40) produces a matrix relationship

$$\boldsymbol{b} = \boldsymbol{S'a} \tag{42}$$

where the entries of the new order-$(NM-1)$ scattering matrix are given by

$$s'_{mn} = S_{mn} + \frac{S_{mi}S_{\text{in}}\Gamma}{1 - S_{ii}\Gamma}. \tag{43}$$

This procedure is repeated, eliminating higher order modes from the scattering matrix, until an $N \times N$ scattering matrix is obtained that relates only the dominant mode interactions.

To summarize, the original $NM \times NM$ generalized S-matrix is reduced by a procedure that modifies the entries of the first $N \times N$ block (representing the dominant mode interactions) to account for the higher order effects. For non-negligible reflection coefficients, the matrix obtained by this procedure is much different from the system that would arise if the $NM \times NM$ system were summarily truncated to order N. However, in the special case when the waveguide apertures are small, and all the higher order modes are substantially cut off, the higher order reflection coefficients will also be quite small, and the first $N \times N$ block of the original system will remain essentially unmodified by the reduction process. Lens designs often utilize small-feed apertures to avoid the possibility of reflected energy reradiating from the feeds, which contributes to ripple in the pattern function and an increase in the sidelobe level. Even in this situation, however, it is necessary to employ higher order modes within each aperture when constructing (24) to properly account for mutual interactions between apertures.

V. Prototype Lens

The numerical formulation was used to test various lens designs, in order to assess the beam pattern and sidelobe level in the presence of mutual coupling between feeds and the specific shape and composition of the lens sidewalls. It was determined that a straight sidewall connecting the beam and array contours [Fig. 4(a)] gave rise to high sidelobes as illustrated in Fig. 4(b). A number of sidewall designs were considered, with a shape such as that illustrated in Fig. 5(a) proving superior. Fig. 5(b) shows the superimposed beam patterns for a lens having sidewall shape shown in Fig. 5(a).

A prototype lens was fabricated for use at 37 GHz containing 34 array ports, 19 beams, and an element spacing of 0.478 cm. The design involved a maximum scan angle of 22.2°, and a focal length of 17.34 cm. The design goal was to achieve −30-dB sidelobes after incorporating a Taylor weighting function. The lens was realized in aluminum using electrical discharge machining techniques. Aluminum plates of 1.0-in thickness each were employed to ensure an overall tolerance specification of ±0.0005 in, and the lens cavity was polished to a surface roughness of 3 μm. Apertures were fed using WR22 rectangular waveguide, with a folded magic-T used to split each feed into two apertures to eliminate the possibility of higher order waveguide modes. The regions along the sidewall [the "ears" in Fig. 5(a)] were lined with absorber material to eliminate reflections. The absorber was type AEMI-20, manufactured by Advanced Electromagnetics, Inc. Figs. 6 and 7 shows the lens interior. Additional details about the magic-T design, the absorber, and the design can be found in [4].

S-parameter measurements were carried out using an HP 8510B network analyzer, an HP 8340B synthesized sweeper, and an HP 8516A test set. The HP 8510B processor was connected through an IEEE 488 interface card to a personal computer, which automated the measurements of S-parameters at 51 frequencies in the 30–40 GHz-band. S-parameters between the 34 array ports and the 19 beam ports were measured in this manner, which provided data for beam patterns and insertion loss. Some S-parameters were also collected to assess the mutual coupling between adjacent and nearly adjacent ports.

Fig. 8 shows the multibeam pattern constructed from the measured S-parameter data at 36.8 GHz, and weighted with a mathematical $(n = 3)$ Taylor weighting function configured to yield −40-dB sidelobes for an ideal $\sin x/x$ pattern. Each beam pattern in Fig. 8 (like Figs. 4(b) and 5(b)) is the pattern

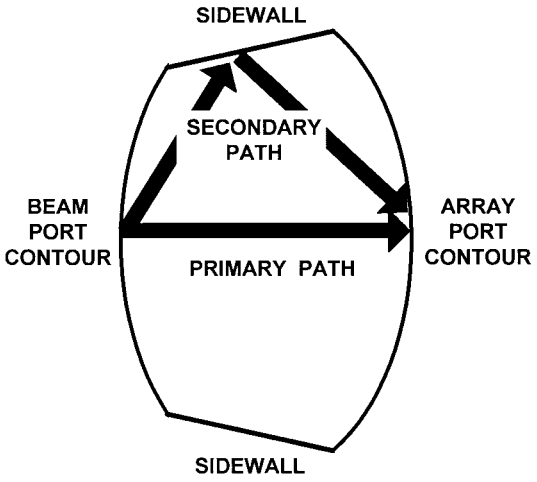

(a)

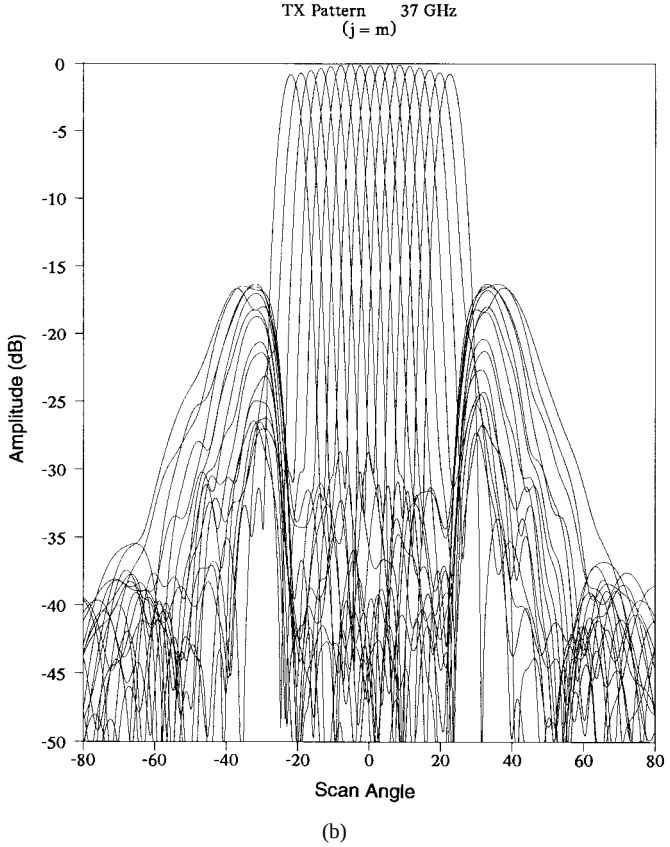

(b)

Fig. 4. (a) Straight sidewall design with possible interference path shown. (b) Beam patterns of lens with straight sidewall design shown in (a). The pattern is a composite with each line representing a single excited beam port, and incorporating a Taylor weighting function configured to yield −40-dB sidelobes in the ideal case.

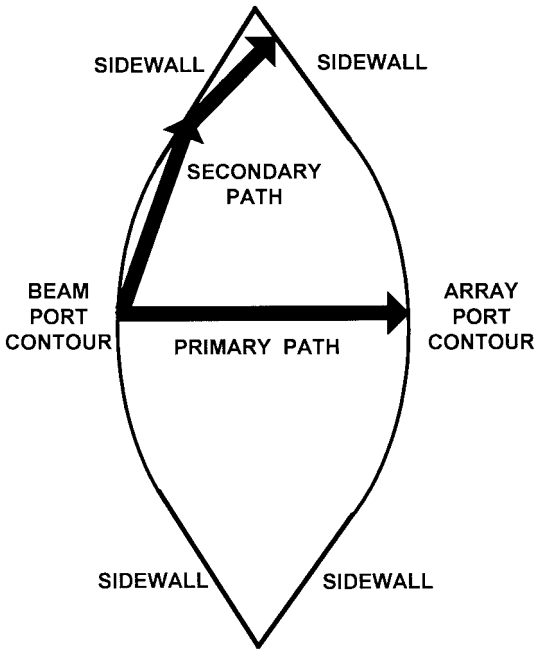

(a)

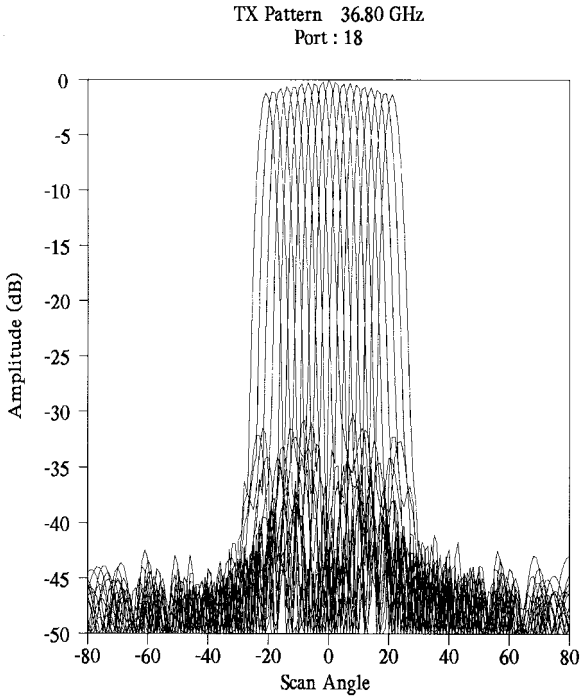

(b)

Fig. 5. (a) Triangular sidewall design. (b) Beam patterns of lens with triangular sidewall design shown in (a). Each line represents the pattern of a single beam port, and incorporates a Taylor weighting function configured to yield −40-dB sidelobes in the ideal case.

associated with one beam port. These patterns are computed from

$$P_k(\theta) = 20 \log_{10} \left| \sum_i W_i S_{ki} e^{-j\phi_{ki}(\theta)} \right|$$

where k denotes a specific beam port and the summation represents the combination of S-parameters from the kth beam port to all the array ports. The phase associated with a particular direction θ is given by

$$\phi_{ki}(\theta) = \frac{2\pi d_i \sin\theta}{\lambda}$$

where d_i is the distance from the center of the antenna array to the ith element, specifically

$$d_i = (0.5)(0.59)(2i+1)\lambda, \qquad \text{where } i = \pm 0,\ 1,\ 2,\ \cdots,\ \pm 15.$$

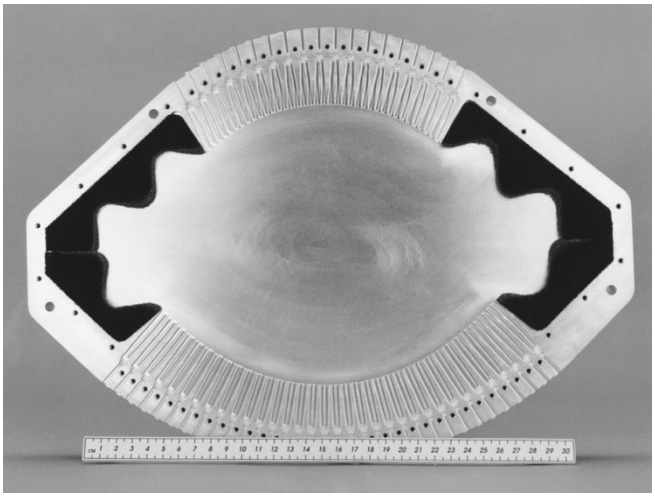

Fig. 6. MMW Rotman lens interior.

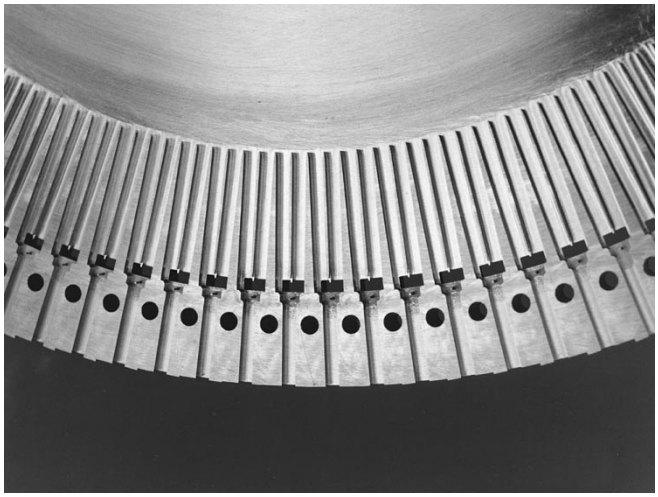

Fig. 7. Magnified lens interior showing magic-T difference ports.

The W are the components of an $(n = 3)$ Taylor weighting function.

VI. Discussion

Although the S-parameter measurements show that the prototype lens meets the desired -30-dB sidelobe specification, the agreement between the numerical and measured results in Figs. 5(b) and 8 is not perfect. The numerical formulation incorporates several assumptions that might account for the lower predicted sidelobe level outside the scan angle. The conducting material is being treated as if it had infinite conductivity, the fields in the rectangular waveguide apertures are assumed to consist of only TE_{1m} modes, and the fields within the parallel-plate region of the lens are assumed to consist only of the TE_1 mode. The treatment of the tapered waveguide transitions neglects the possible conversion of one mode into another, and the magic-T junctions are assumed to have ideal characteristics. When using an impedance boundary condition to model the absorbing material located in the sidewall region, we were forced to estimate the impedance from the far-field reflection properties [4] since we did not know the exact

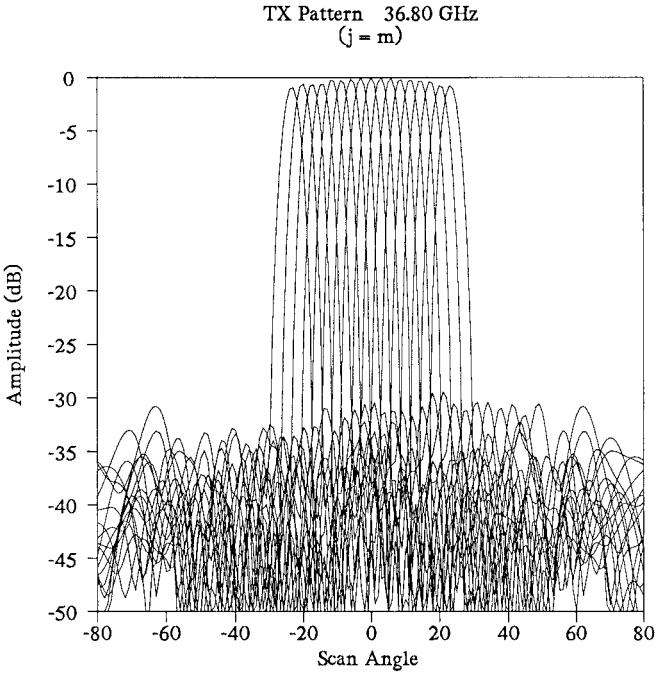

Fig. 8. Composite beam patterns at 36.8 GHz, obtained from measured S-parameter data for the lens shown in Figs. 1 and 6. The S-parameters were modified with an ideal $(n = 3)$ Taylor weighting function configured to yield -40-dB sidelobes in order to generate the beam patterns.

materials used in the absorber. Studies suggested that a similar absorbing effect could be obtained using dummy apertures backed by tapered lines terminated in matched loads to model that portion of the lens contour. Fig. 5(b) was produced using dummy apertures instead of an impedance condition.

Appendix
Expressions for Aperture to Aperture Coupling

Source/field relations can be derived using standard procedures [13]. The specific approach developed in this paper only required two expressions: The z-component of the magnetic field (H_z) in the parallel-plate lens cavity due to a transverse equivalent electric current J_t, and H_z due to a z-component of equivalent magnetic current M_z. These expressions are

$$hzjt^p_{qm}(u) = -\int_{t=0}^{w^q} \cos\left(\frac{m\pi t}{w^q}\right) \cdot \left\{\cos\phi^q \frac{\Delta X}{R} + \sin\phi^q \frac{\Delta Y}{R}\right\} \frac{k_{pp}}{4j} H_1^{(2)}(k_{pp}R)\,dt \quad \text{(A.1)}$$

$$hzmz^p_{qm}(u) = \frac{k_{pp}^2}{j\omega\mu} \int_{t=0}^{w^q} \cos\left(\frac{m\pi t}{w^q}\right) \frac{1}{4j} H_0^{(2)}(k_{pp}R)\,dt \quad \text{(A.2)}$$

where

$$\Delta X = x - x'(t) = x - x'(0) + t\sin\phi \quad \text{(A.3)}$$

$$\Delta Y = y - y'(t) = y - y'(0) - t\cos\phi \quad \text{(A.4)}$$

$$R = \sqrt{\Delta X^2 + \Delta Y^2}. \quad \text{(A.5)}$$

R is the distance between the observer $(x[u], y[u])$ in aperture p and the point of integration $(x'[t], y'[t])$ in aperture q, with

the integration expressed in terms of the local variable t. The source aperture q is oriented with a tangent vector defined in terms of a conventional cylindrical coordinate variable ϕ

$$\hat{t} = -\hat{x}\,\sin\,\phi + \hat{y}\,\cos\,\phi. \tag{A.6}$$

The actual calculations involve an integration over the observer aperture p, and we introduce a local integration variable u in aperture q in order to write

$$\begin{aligned} hzjt_{qm}^{pv} = &-\int_{u=0}^{w^p} \cos\left(\frac{v\pi u}{w^p}\right) \int_{t=0}^{w^q} \cos\left(\frac{m\pi t}{w^q}\right) \\ &\cdot \left\{\cos\,\phi^q \frac{\Delta X}{R} + \sin\,\phi^q \frac{\Delta Y}{R}\right\} \frac{k_{pp}}{4j} H_1^{(2)} \\ &\cdot (k_{pp}R)\,dt\,du \end{aligned} \tag{A.7}$$

and

$$\begin{aligned} hzmz_{qm}^{pv} = &\frac{k_{pp}^2}{j\omega\mu} \int_{u=0}^{w^p} \cos\left(\frac{v\pi u}{w^p}\right) \int_{t=0}^{w^q} \\ &\cdot \cos\left(\frac{m\pi t}{w^q}\right) \frac{1}{4j} H_0^{(2)}(k_{pp}R)\,dt\,du. \end{aligned} \tag{A.8}$$

Except in the case when $p = q$, these expressions can be evaluated by conventional numerical quadrature. When $p = q$, the variable R vanishes within the interval of integration, and the singularities of the Hankel functions at the origin complicate the numerical evaluation. Equation (A.7) can be evaluated by a limiting procedure, while (A.8) can be evaluated by either extracting the logarithmic singularity, or by using a quadrature rule that incorporates the logarithmic singularity. All three procedures are fairly well known and are described in [13].

REFERENCES

[1] W. Rotman and R. F. Turner, "Wide-angle microwave lens for line source application," *IEEE Trans. Antennas Propagat.*, vol. AP-11, pp. 623–632, Nov. 1963.

[2] D. R. Gagnon, "Procedure for correct refocusing of the Rotman lens according to Snell's law," *IEEE Trans. Antennas Propagat.*, vol. 37, pp. 390–392, Mar. 1989.

[3] R. C. Hansen, "Design trades for Rotman lenses," *IEEE Trans. Antennas Propagat.*, vol. 39, pp. 464–472, Apr. 1991.

[4] O. Rausch, J. Sexton, G. Hampton, M. Kapa, K. Murphy, M. Cole, and A. F. Peterson, "The development and modeling of a millimeter wave Rotman lens," Georgia Institute of Technology, Final Rep. for U.S. Army Res. Lab. AMSRL-SE-RM, Sept. 1996.

[5] D. M. Pozar, *Microwave Engineering.* New York: Wiley, 1998.

[6] T. Okoshi and T. Miyoshi, "The planar circuit—An approach to microwave integrated circuitry," *IEEE Trans. Microwave Theory Tech.*, vol. MTT-20, pp. 245–252, 1972.

[7] T. Okoshi, *Planar Circuits for Microwave and Lightwaves.* Berlin, Germany: Springer-Verlag, 1985.

[8] K. K. Chan, "Field analysis of planar bootlace lens feeds," in *Proc. Int. Radar Conf.*, Paris, France, 1989, pp. 273–278.

[9] P. C. Sharma, K. C. Gupta, C. M. Tsai, J. D. Bruce, and R. Presnell, "Two-dimensional field analysis for CAD of Rotman-type beam-forming lenses," *Int. J. Microwave and Millimeter-Wave Computer-Aided Eng.*, vol. 2, pp. 90–97, Apr. 1992.

[10] A. F. Peterson and E. O. Rausch, "Validation of integral equation model with high-dielectric Rotman lens measurements," in *Proc. 1991 Antenna Applications Symp.*, Monticello, IL, Sept. 1991, pp. 208–229. These proceedings are available as Tech. Rep. RL-TR-92-42, Rome Lab., Griffiss Air Force Base, NY, Feb. 1992.

[11] E. O. Rausch, A. Erbil, H. M. Harris, R. L. Moore, T. B. Wells, D. C. Wilburn, and A. F. Peterson, "The development and modeling of a compact high-dielectric Rotman lens," Wright Lab. Tech. Rep. WL-TR-92-1112, Wright-Patterson Air Force Base, OH, July 1992.

[12] E. O. Rausch and A. F. Peterson, "Theory and measurements of a compact high dielectric microstrip Rotman lens," in *Proc. 22nd European Microwave Conf.*, Espoo, Finland, Aug. 1992, pp. 876–881.

[13] A. F. Peterson, S. L. Ray, and R. Mittra, *Computational Methods for Electromagnetics.* New York: IEEE Press, 1998.

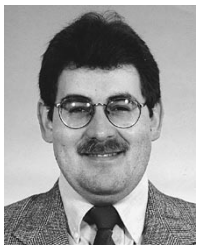

Andrew F. Peterson (S'82–M'83–SM'92) received the B.S., M.S., and Ph.D. degrees in electrical engineering from the University of Illinois, Urbana-Champaign, in 1982, 1983, and 1986, respectively.

Since 1989, he has been a member of the faculty of the School of Electrical and Computer Engineering, Georgia Institute of Technology, Atlanta, where he is now a Professor. He teaches electromagnetic field theory and computational electromagnetics, and conducts research in the development of computational techniques for electromagnetic scattering, microwave devices, and electronic packaging applications. He is the principal author of the text *Computational Methods for Electromagnetics*, IEEE Press, 1998.

Dr. Peterson is a past recipient of the ONR Graduate Fellowship and the NSF Young Investigator Award. He has served as an Associate Editor of the IEEE TRANSACTIONS ON ANTENNAS AND PROPAGATION, as Chairman of the Atlanta joint IEEE AP-S/MTT chapter, and as the General Chair of the 1998 IEEE AP-S International Symposium and URSI/USNC Radio Science Meeting. He has also served for six years as a Director of ACES and is currently a member of AP-S AdCom. He is a member of ACES, URSI Commission B, IMAPS, ASEE, and AAUP.

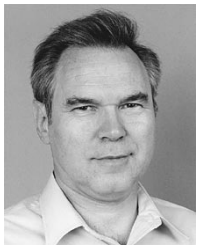

Ekkehart O. Rausch received the M.S. and Ph.D. degrees in physics from the Georgia Institute of Technology, Atlanta. He completed a postdoctoral fellowship on the development of a surface analysis technique using ion implantation and sputtering techniques.

Since 1989, he has been employed at the Georgia Tech Research Institute, a unit of the Georgia Institute of Technology. At the present time, he is associated with the Sensors and Electromagnetic Applications Laboratory. He is currently classified as a Senior Research Scientist and conducts research in the areas of antennas, fiber optics, and electronic protection of radars. In the field of antennas, he specializes in the development of Rotman lenses in the millimeter-wave region. He is credited with more than 50 publications.